

# Measurement of the Casimir-Polder force through center-of-mass oscillations of a Bose-Einstein condensate

D. M. Harber, J. M. Obrecht, J. M. McGuirk,\* and E. A. Cornell†

*JILA, National Institute of Standards and Technology and University of Colorado Department of Physics,  
University of Colorado, Boulder, Colorado 80309-0440*

(Dated: November 9, 2018)

We have performed a measurement of the Casimir-Polder force using a magnetically trapped  $^{87}\text{Rb}$  Bose-Einstein condensate. By detecting perturbations of the frequency of center-of-mass oscillations of the condensate perpendicular to the surface, we are able to detect this force at a distance  $\sim 5\ \mu\text{m}$ , significantly farther than has been previously achieved, and at a precision approaching that needed to detect the modification due to thermal radiation. Additionally, this technique provides a limit for the presence of non-Newtonian gravity forces in the  $\sim 1\ \mu\text{m}$  range.

PACS numbers: 03.75.Kk, 34.50.Dy, 31.30.Jv, 04.80.Cc

## I. INTRODUCTION

Interest in the Casimir-Polder [1] force, the attractive QED force between an atom and a surface, and the closely related Casimir force, the attractive QED force between two surfaces, has blossomed in recent years following the breakthrough experiments of Sukenik *et al.* [2] and Lamoreaux [3]. Additionally, the tremendous experimental progress in both ultracold atomic systems and microelectromechanical systems (MEMS's), has pushed both fields towards precise work very close to surfaces—regimes where Casimir-type effects become important.

To the present, experiments have identified the crossover in behavior between the van der Waals-London and Casimir-Polder regimes, which occurs at an atom-surface separation of  $\sim 0.1\ \mu\text{m}$  for  $^{87}\text{Rb}$ . Inside of this crossover, the van der Waals-London regime, the potential scales as  $1/d^3$ , where  $d$  is the distance between the atom and surface. Outside of this crossover, the Casimir-Polder regime, the potential scales as  $1/d^4$ . It has been predicted that the presence of thermal radiation from the surface and surroundings will modify the behavior of this force. This modification is predicted to occur at even greater atom-surface separations, i.e.  $\sim 7\ \mu\text{m}$  at 300 K. In this large-separation regime, hereafter referred to as the thermal regime, the potential scales as  $T/d^3$ , where  $T$  is the temperature of the thermal blackbody.

The experiment of Sukenik *et al.* [2] was the first to clearly measure the crossover from the van der Waals-London to the Casimir-Polder regime. A number of experiments followed that used ultracold atoms to detect the presence of the Casimir-Polder force [4, 5, 6, 7, 8, 9]; however, none have approached the sensitivity at large distances required to detect a crossover to the thermal regime.

Perhaps the most obvious technique for measurements of surface forces using ultracold atoms is interferometry in which atoms take separate spatial paths. This sort of atom interferometry has proved difficult, but some groups have now started to make headway in this direction [10, 11, 12].

In this experiment, the effects of the surface potential on the *mechanical* motions of a Bose-Einstein condensate are studied. The attractive surface force distorts the trapping potential and thus manifests itself in a number of ways. First, the center-of-mass position of the atoms changes, but only by  $\sim 10\ \text{nm}$  for our 228 Hz trapping potential when the condensate is several microns from the surface. Position deviations on this order are well below our experimental sensitivity; thus, detection of the Casimir-Polder force in this manner is unfeasible. Second, the collective oscillation frequencies of the condensate change. Of these, the center-of-mass oscillation, or dipole oscillation, is perhaps the most robust because it is very long lived and its frequency is independent of intracondensate interactions.

In the most simple approximation, the normalized dipole oscillation frequency shift in the  $\hat{x}$  direction [see Fig. 1(a)], hereafter referred to as  $\gamma_x$ , can be written as

$$\gamma_x \equiv \frac{\omega_x - \omega'_x}{\omega_x} \simeq -\frac{1}{2\omega_x^2 m} \partial_x^2 U^*, \quad (1)$$

where  $\omega_x$  is the unperturbed trap frequency in the  $\hat{x}$  direction,  $\omega'_x$  is the perturbed trap frequency,  $m$  is the mass of  $^{87}\text{Rb}$ ,  $\partial_x^2$  is the second partial derivative with respect to  $x$ , and  $U^*$  is the potential experienced by the atoms due to the surface. Thus the dipole oscillation frequency is sensitive to the second derivative of the potential, or to force *gradients*.

A detailed theoretical analysis of this system was performed by Antezza *et al.* [13]. This analysis includes a careful calculation of the Casimir-Polder force from a dielectric surface, the modification to the Casimir-Polder force in the thermal regime, and the expected normalized dipole frequency shift  $\gamma_x$ , taking into account the finite width of the condensate and the finite oscillation amplitude. The result of this analysis is that for experimentally plausible conditions, the expected values of  $\gamma_x$  are on the order of  $10^{-4}$ , well within experimental precision.

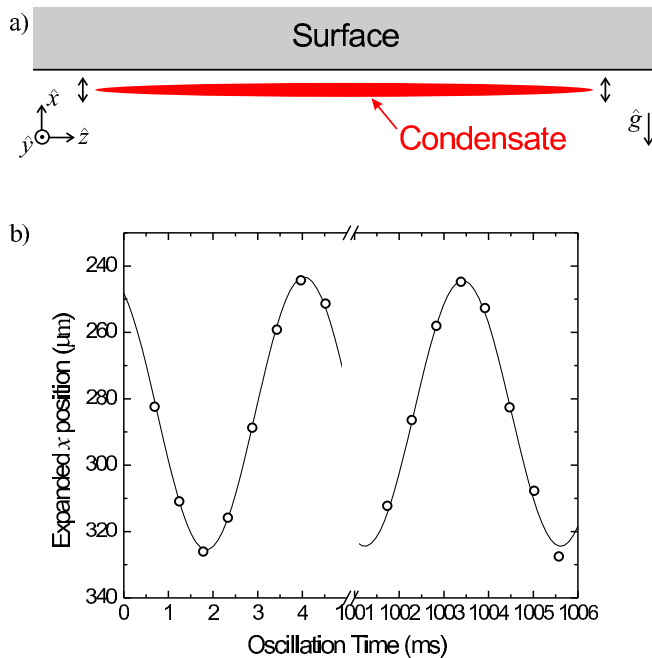


FIG. 1: (Color online) (a) Diagram, to scale, illustrating the aspect ratio of the condensate and typical oscillation position relative to the surface. The coordinate axis orientation and the direction of gravity are also indicated. (b) Typical data showing the radial dipole oscillation after expansion away from the surface.

## II. EXPERIMENT

We briefly review the apparatus for generating condensates and measuring surface forces, as a more detailed description of the apparatus used to produce the condensate can be found in [14] and the technology and techniques for atom-surface measurements are described in detail in [15, 16]. At the end of evaporation, nearly pure condensates (the fraction of atoms in the condensate  $\geq 0.8$ ) of  $1.4 \times 10^5$  magnetically trapped  $^{87}\text{Rb}$  atoms are created in the  $|F = 1, m_F = -1\rangle$  ground state. In our Ioffe-Pritchard-type magnetic trap, with trapping frequencies of 6.4 Hz in the axial direction ( $\hat{z}$ ) and 228 Hz in the radial directions ( $\hat{x}$  and  $\hat{y}$ ), this corresponds to condensate Thomas-Fermi radii of 85.9  $\mu\text{m}$  and 2.40  $\mu\text{m}$  in the axial and radial directions, respectively. See Fig. 1(a) for the coordinate definitions and orientations of the surface and condensate in the experiment.

The surfaces for study are located  $\sim 1$  mm above ( $+\hat{x}$  direction) where evaporation occurs. To position the condensate near the surface, a vertical ( $\hat{x}$  direction) magnetic field is applied. This uniform magnetic field acts to displace the magnetic minimum of the trapping field. By applying a carefully controlled field ramp, we are able to move the atoms arbitrarily close to the surface without exciting mechanical oscillations of the condensate, and the condensate can be held there for many seconds.

To measure the distance between the condensate and

the surface, we use an absorption imaging technique described in [15, 17] where we illuminate the atoms with a beam perpendicular to the long axis of the condensate. This beam impinges on the surface with a slight grazing incidence angle of  $\sim 2.4^\circ$  such that when the condensate is within  $\sim 100 \mu\text{m}$  of the surface, both a direct absorption image and a reflected absorption image of the condensate appear. Measuring the distance between these images allows us to determine the distance between the condensate and surface. To calibrate the magnetic field necessary to position the condensate a given distance from the surface, a series of images are taken where we push the atoms to a range of distances  $\sim 20\text{--}60 \mu\text{m}$  from the surface. The condensate-surface separations in these images are measured and then used for calibration of the magnetic field used to push the atoms.

To allow measurement of surface forces at different surface locations, the magnetic trap can be moved independently of the surface in the  $\hat{y}$  and  $\hat{z}$  directions. Since the condensate only interacts with a  $\sim 200 \times 10 \mu\text{m}$  region of the surface, we can translate the trap to measure surface forces at many different locations on our  $5 \times 8$  mm surfaces. Finally, we can adjust the angle of the  $\hat{z}$  trap axis to be parallel with respect to the surfaces. Using the surface reflection images, we have verified that the deviation from parallel is  $\leq 0.25^\circ$ .

To excite a condensate dipole oscillation in the  $\hat{x}$  direction, we apply an oscillating magnetic field of the form

$$B_x(t) \propto e^{-(t-t_0)^2/\tau^2} \cos(\omega_x t), \quad (2)$$

where  $\tau$  is the time width of the pulse (10 ms in this experiment) and  $t_0$  is the time of the peak of the pulse. In frequency space, this excitation is centered on the radial trap frequency  $\omega_x$  and contains no dc or high-frequency components; this prevents excitation of unwanted internal condensate modes. Similarly, dipole oscillations can be excited in the  $\hat{y}$  and  $\hat{z}$  directions.

Expansion of the oscillating condensate is accomplished by a microwave adiabatic rapid passage to the  $|F = 2, m_F = -2\rangle$  state, which is antitrapped, followed by  $\sim 5$  ms of rapid antitrapped expansion [14]. The antitrapped expansion acts to push atoms away from the magnetic minimum, and because of gravitational sag, the condensate begins the expansion below the magnetic minimum, so the condensate is pushed away from the surface during expansion. Additionally, the antitrapped expansion acts to amplify the radial dipole oscillation amplitude by approximately 20-fold, permitting straightforward measurement of the oscillation in expansion. For example, see Fig. 1(b). Finally, the condensate is simultaneously imaged through absorption along both the  $\hat{y}$  and  $\hat{z}$  directions, allowing us to monitor the position of the condensate in all three directions.

The typical experiment is performed as follows. First, a surface calibration set is taken to determine the magnetic field necessary to position the condensate the desired distance from the surface. Second, a vertical os-

cillation data set is taken at the desired trap-center to surface distance  $d$ , typically 6–12  $\mu\text{m}$ . Interspersed with these data are vertical oscillation data taken at  $d_0$ , the distance we use to obtain the normalization frequency  $\omega_x$ . Data points and normalization points were randomly alternated during the course of the data set in order to prevent trap frequency drift from affecting our measurement. For this experiment  $d_0 = 15 \mu\text{m}$ . A distance of 15  $\mu\text{m}$  is far away enough such that surface forces will not affect the frequency; the normalized dipole frequency shift from the Casimir-Polder force is less than  $10^{-6}$  at this distance. By comparing the frequency measured at  $d$  to that measured at  $d_0$ , we obtain  $\gamma_x$  at the particular condensate-surface separation  $d$ . Last, a second surface calibration set is taken to determine the condensate-surface distance drift over the course of the data set, typically  $\ll 1 \mu\text{m}$ .

### III. SYSTEMATICS

Rejection of the presence of spurious forces on the condensate caused by surface-based electric and magnetic fields is critical to the interpretation of our results. Our most powerful test for spurious forces is provided by the elongated geometry of our condensate. The mean condensate-surface separation for our closest measurements,  $\sim 6 \mu\text{m}$ , is significantly smaller than the axial extent of the condensate,  $\sim 170 \mu\text{m}$  [see Fig. 1(a)]. Thus a spatially inhomogeneous force, due to localized electric or magnetic surface contamination, would likely affect only part of the condensate. When oscillating in this inhomogeneous potential, the condensate behaves more like a string than a stiff bar and thus will oscillate at different radial frequencies along its axial extent. Using a technique fully described in [16], we analyze images of the oscillating condensate and obtain  $\gamma_x(z)$  axially along the center  $\sim 120 \mu\text{m}$  of the condensate, in addition to  $\gamma_x^{cm}$  for the center of mass of the condensate.

To investigate the presence of a spatially inhomogeneous force, we examine  $\gamma_x(z)$  across the condensate. We first define the standard deviation of  $\gamma_x(z)$  along the axial extent of the condensate to be  $\delta_\gamma$ . If  $\delta_\gamma$  is greater than a predefined threshold value [18], then we surmise that there is a statistically significant spatially inhomogeneous force acting on the condensate and thus move to a new surface location. On the other hand, if  $\delta_\gamma$  is less than the threshold value, then we take  $\delta_\gamma$  to be our systematic limit on spatially inhomogeneous forces experienced by the condensate.

Spatially uniform spurious shifts along the extent of the condensate are less likely but must also be accounted for. A completely uniform surface charge, or magnetization, will by symmetry not generate a force. The remaining possible cause of spurious uniform forces is then stripes of surface contaminations collinear with the axis of the condensate [19]. To test for this possibility, we perform measurements at multiple surface locations, as

well as a series of measurements to test for the presence of magnetic and electric fields.

An atom in an electric field will experience an energy shift according to  $U_E = -(\alpha_0/2)E^2$ , where  $\alpha_0$  is the ground-state dc polarizability and  $E$  is the electric field magnitude. Thus, to first approximation, the normalized frequency shift caused by an electric field can be written as

$$\gamma_x \propto -\partial_x^2 U_E = \frac{\alpha_0}{2} \partial_x^2 [(E_x^*)^2 + (E_y^*)^2 + (E_z^*)^2]. \quad (3)$$

Our goal is then to determine the  $x$  dependence of the surface electric fields  $E_x^*$ ,  $E_y^*$ , and  $E_z^*$ ; from these we can obtain an estimate of  $\gamma_x$ . In our previous work [16], we applied a uniform dc external electric field  $E_x^{ext}$ , and by measuring a change in  $\gamma_x$  as  $E_x^{ext}$  was varied  $\pm 100 \text{ V/cm}$ , we were able to obtain  $\partial_x^2 E_x^*(x)$ . For the current work, we are instead using a technique that allows us to measure  $\partial_x E_x^*(x)$  as well as  $\partial_x E_y^*(x)$  and  $\partial_x E_z^*(x)$ .

If rather than apply a dc external electric field we apply an ac external electric field  $E_x^{ext} \cos(\omega t)$ , where  $E^{ext} \gg E^*$ , and we invoke  $\vec{\nabla} \times \vec{E} \simeq 0$  [20], then the forces on the atoms are

$$F_x(t) \simeq \alpha_0 E_x^{ext} \cos(\omega t) \partial_x E_x^*, \quad (4)$$

$$F_y(t) \simeq \alpha_0 E_x^{ext} \cos(\omega t) \partial_x E_y^*, \quad (5)$$

$$F_z(t) \simeq \alpha_0 E_x^{ext} \cos(\omega t) \partial_x E_z^*. \quad (6)$$

If  $\omega$  is set to  $\omega_x$ ,  $\omega_y$ , or  $\omega_z$  and  $\partial_x E_{x,y,z}^*$  is nonzero, then the oscillating electric field will resonantly drive a dipole oscillation. This allows the measurement of very small electric forces. By keeping the drive time short, 50–100 ms in our experiment, compared to the oscillation damping rate, typically 1–10 s, and the inverse of the drive detuning, typically  $< 0.5 \text{ Hz}$ , then the system reduces to that of an undamped, resonantly driven oscillator. In this case, the oscillation amplitude linearly grows as

$$\dot{A} = \frac{F_0}{2\omega m}, \quad (7)$$

where  $F_0$  is the amplitude of the driving force and  $\dot{A}$  is the rate of growth of the amplitude. By positioning the condensate at a given distance from the surface and driving a large external electric field ( $\sim 100 \text{ V/cm}$ ) at the  $\hat{i}$  trap frequency, we are able to detect  $\partial_x E_i^*$ , where  $\hat{i}$  represents the  $\hat{x}$ ,  $\hat{y}$ , or  $\hat{z}$  direction. This measurement is performed at multiple distances from the surface, and  $\partial_x E_i^*(x)$  is fit to a form  $\partial_x E_i^*(x) = -p_i C_i / x^{p_i+1}$ . This corresponds to an electric field of the form  $E_i^*(x) = C_i / x^{p_i}$ . When fitting this data for  $C_i$  we vary the exponent  $p_i$  between 0.20, corresponding to a very broad collinear surface charge or dipole distribution, and 2.0, corresponding to a line of dipoles. Finally, using this range of powers, the power-law fit leading to the largest systematic error is used.

Although less prevalent, evidence of magnetic surface contaminants can be seen on our insulating surface (likely remnants from surface polishing). Our trapping potential itself is magnetic, so we cannot rely on techniques similar to those used for the detection of electric fields. Instead, we carefully examine the magnetic trapping potential itself. A spurious magnetic field cannot exclusively modify  $\omega_x$ ; rather, the spurious field will manifest itself as a modification of multiple trapping frequencies, or anomalous center-of-mass displacements.

The trap frequencies in the three directions can be expressed as

$$\omega_x = \omega_y = \sqrt{\frac{\mu_B m_F g_F}{m}} \frac{\eta}{\sqrt{B_0}}, \quad (8)$$

$$\omega_z = \sqrt{\frac{\mu_B m_F g_F}{m}} \sqrt{\beta}, \quad (9)$$

where  $\mu_B$  is the Bohr magneton,  $g_F$  is the Landé  $g$  factor,  $\eta$  is the linear magnetic field gradient in the  $\hat{x}$  and  $\hat{y}$  directions [21],  $B_0$  is the bias field, and  $\beta$  is the magnetic field curvature in the  $\hat{z}$  direction [ $B_z(z) = B_0 + \beta/2 z^2$ ]. Adding an additional spurious magnetic field  $B^*$  and expanding to first order in  $B^*$ , the normalized frequency shift  $\gamma_{x,y,z}$  induced by the spurious magnetic field can be written as

$$\gamma_x = \frac{B_z^*}{2B_0} - \frac{\partial_x B_x^*}{\eta} - \frac{B_0 \partial_x^2 B_z^*}{2\eta^2}, \quad (10)$$

$$\gamma_y = \frac{B_z^*}{2B_0} + \frac{\partial_y B_y^*}{\eta} - \frac{B_0 \partial_y^2 B_z^*}{2\eta^2}, \quad (11)$$

$$\gamma_z = -\frac{\partial_z^2 B_z^*}{2\beta}. \quad (12)$$

Invoking  $\vec{\nabla} \cdot \vec{B}^* = 0$  and  $\vec{\nabla} \times \vec{B}^* \simeq 0$  [22], we obtain an expression for the systematic uncertainty in the normalized frequency shift caused by a spurious magnetic field,  $\delta\gamma_x$ , as

$$\delta\gamma_x \simeq \sqrt{(\delta\gamma_y)^2 + \frac{B_0^2 \beta^2}{\eta^4} (\delta\gamma_z)^2 + \frac{\beta^2}{\eta^2} (\delta z_{cm})^2}, \quad (13)$$

where we have introduced  $\delta\gamma_y$  and  $\delta\gamma_z$ , which are the measured systematic limits on deviations from zero of  $\gamma_y$  and  $\gamma_z$  as the condensate nears the surface, and  $\delta z_{cm}$ , which is the uncertainty in the movement of the center of mass of the condensate in the  $\hat{z}$  direction from its equilibrium position.

This technique can be summarized as follows. If the only force on the condensate is the Casimir-Polder force, then  $\gamma_y$ ,  $\gamma_z$ , and  $z_{cm}$  will not change as the condensate is moved near the surface. Therefore, if  $\gamma_y$ ,  $\gamma_z$ , and  $z_{cm}$  display no statistically significant deviation, then we have verified that magnetic forces from the surface are not present at measurable levels. The uncertainty in these

TABLE I: A summary of our errors in  $\gamma_x$ . The  $1\sigma$  error bars in Fig. 2 represent a combination of statistical and systematic errors. The relative contributions of the various sources of statistical and systematic error were evaluated separately for each point. Values for the errors for the worst point and for a typical point are tabulated under "Maximum" and "Typical" below.

Error source	Maximum ( $10^{-5}$ )	Typical ( $10^{-5}$ )
Statistical	8.3	4.0
Spatial inhomogeneity	4.6	2.5
Uniform magnetic	2.9	2.2
Uniform electric	4.1	0.41
Normalization	0.18	0.14
Total	-	5.2

terms,  $\delta\gamma_y$ ,  $\delta\gamma_z$ , and  $\delta z_{cm}$ , then allow us to obtain a systematic limit on the presence of magnetic forces.

This technique, where we only consider uncertainties of fields, is not applicable in the case of the electrical systematics because typically a nonzero electric field is detected. Therefore, the perturbation of the measured electric field, rather than the uncertainty in the presence of an electric field, dominates the electrical systematics.

Finally, we acknowledge that in certain situations, a magnetic field could cause a change in  $\gamma_x$  and no change in  $\gamma_y$ —for instance, if  $B_z^*/(2B_0) = -\partial_y B_y^*/\eta$ . Unlikely situations such as this cannot be categorically excluded with our current analysis technique; however, by performing measurements at multiple surface locations and verifying that these measurements agree, we can reduce the possibility that this sort of unusual cancellation could disturb our measurement.

## IV. RESULTS

The surfaces with which these experiments were performed were  $\sim 8 \times 5 \times 2$  mm<sup>3</sup> pieces of UV-grade fused silica and sapphire polished to  $\sim 0.5$  nm surface roughness. Conducting surfaces would in some way be preferable, largely because they are less susceptible to electric fields caused by surface charge. Unfortunately, alkali-metal atoms, when adsorbed on a conducting surface, generate a significant electric dipole field [16]. Preventing any atoms from striking the surface during a measurement is unfeasible, so it seems that dielectric surfaces, despite the possible presence of surface charges, are preferable in this case.

The dielectric surfaces studied include (1) UV-grade fused silica prepared by a hydrofluoric acid etch followed by UV-ozone cleaning, (2) sapphire prepared with UV-ozone cleaning, and (3) UV-grade fused silica cleaned with acetone, ultrapure methanol, and de-ionized water. Surfaces (1) and (2) displayed forces that were 3–10 times

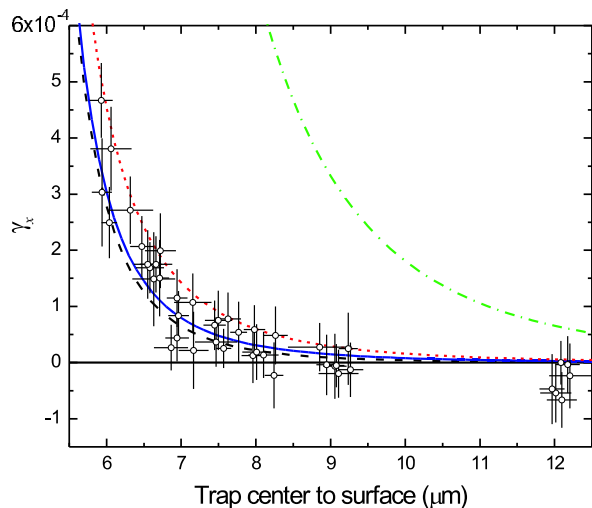


FIG. 2: (Color online) Normalized frequency shift data from the fused silica surface (dc dielectric constant = 3.83 [23]). Each data point represents a single measurement of  $\gamma_x$  (no data averaging was performed). These data were taken at two locations spaced  $300\ \mu\text{m}$  apart. Vertical error bars include the statistical and systematic errors detailed in Table I. Horizontal error bars include statistical uncertainty, surface drift, and the effects of the uncertainty in the image magnification. For this data set the mean oscillation amplitude, including the small effects of damping, is  $2.06\ \mu\text{m}$ . The mean Thomas-Fermi radius in the  $\hat{x}$  direction is  $2.40\ \mu\text{m}$  for this data. Theory lines, calculated using the theory from Antezza *et al.* [13, 24], indicate  $T = 0\text{ K}$  (dashed, black line),  $T = 300\text{ K}$  (solid, blue line), and  $T = 600\text{ K}$  (dotted, red line). Additionally we include the extrapolation of the van der Waals-London  $1/d^3$  potential to these distances (dash-dotted, green line).

larger than the Casimir-Polder force and displayed significant spatial inhomogeneity. Previous studies of a BK7 surface had led us to believe that magnetic impurities embedded during the polishing process were a problem, thus leading us to try an aggressive surface preparation such as a hydrofluoric acid etch. However, with our current surfaces, spurious forces appear to be primarily caused by spatially inhomogeneous electric surface potentials.

The fused silica surface (3) displayed the smallest level of spurious forces. Nevertheless, even with this surface we were forced to study multiple spatial locations in order to locate suitable positions for measurements. Suitable locations were primarily identified by the criteria that  $\delta_\gamma$  be less than a certain predefined threshold value. Approximately 40% of the surface regions studied displayed spatially inhomogeneous forces. The spatially inhomogeneous forces, identified with the technique previously described, displayed peak values  $\sim 100\%$  larger than the Casimir-Polder force. Spatial variations occurred on  $\sim 50\ \mu\text{m}$  distance scales and displayed  $\sim 100\%$  percent variations in strength. It is possible that finer structure could be present, yet not detectable.

Once a suitable region was identified, we performed the

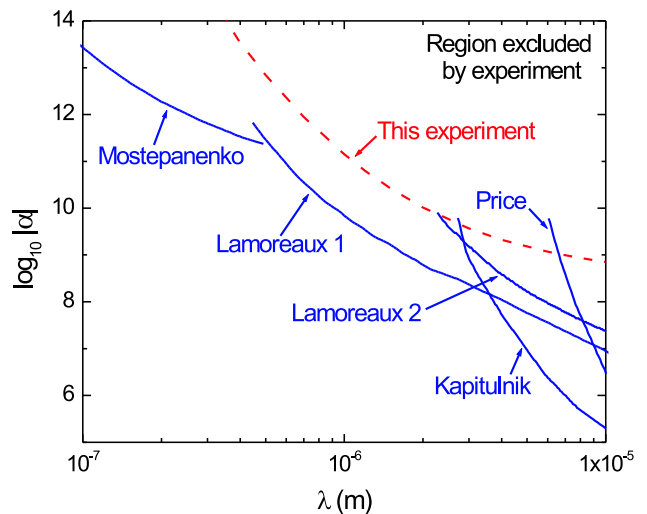


FIG. 3: (Color online) Current short-range Yukawa-type force limits in the  $0.1\text{--}10\ \mu\text{m}$  range. The limits obtained from this experiment are shown by the dashed line. The limits labeled Mostepanenko, Kapitulnik, and Price are from [26], [27], and [28], respectively. The limits labeled Lamoreaux (a) and (b), from [29] and [30], respectively, are from two different analyses of the Lamoreaux experiment [3].

experimental procedure previously outlined to measure  $\gamma_x$ . In addition, a significant amount of data was concurrently taken to put limits on spatially uniform electric and magnetic forces. Table I summarizes the limits from these systematic measurements. The results of our measurement of the Casimir-Polder force from surface (3) are shown in Fig. 2.

The first thing to note is that our measurement distances are deep within the retarded, or Casimir-Polder, regime. This is highlighted by the profound disagreement between the measured force and the extrapolation of the van der Waals-London force to this distance regime, as shown in Fig. 2. We do, on the other hand, see good agreement with the predicted Casimir-Polder force from our fused silica surface. Unfortunately, we currently do not have the experimental resolution to discern between the  $T = 0\text{ K}$  Casimir-Polder force and the  $T = 300\text{ K}$  case. Repeating the measurement at an elevated temperature, however, appears promising; see Fig. 2 for the prediction for  $T = 600\text{ K}$ . At this temperature, the predicted  $\gamma_x$  is larger than nearly all of our data; thus a measurement repeated at this temperature should yield a significantly larger signal. Additionally, observation of a direct correlation between a change in temperature and a corresponding increase the Casimir-Polder force would clearly demonstrate the thermal regime of the Casimir-Polder force.

If we assume the  $T = 300\text{ K}$  Casimir-Polder theory is correct, then the data in Fig. 2 can additionally be used to put limits on short-range scalar-scalar Yukawa potentials of the type [25]

$$U_{Yuk} = - \int dV \frac{Gm\rho}{r} (1 + \alpha e^{-r/\lambda}), \quad (14)$$

where  $G$  is the Newtonian constant of gravitation,  $m$  is the mass of rubidium,  $\rho$  is the density of the attracting body (in our case the fused silica substrate),  $r$  is the distance from the rubidium atom to the volume element in the substrate,  $\alpha$  and  $\lambda$  parametrize the short-range Yukawa force, and the volume integral is performed over the fused silica substrate.

For each value of  $\lambda$ , we increase a hypothetical  $\alpha$  until the value of the  $\gamma_x$  predicted due to the hypothetical Yukawa force plus the predicted  $T = 300$  K Casimir-Polder force is excluded at the 95% level by the data as shifted by worst-case assumptions on the systematics (for this analysis uncertainties in spurious magnetic forces dominate). The limit obtained in this manner is plotted in Fig. 3 with the current experimental limits in this region. Redesigning the experiment to optimize sensitivity to this signal could permit over an order-of-magnitude improvement in the short-range force sensitivity. This improvement could be accomplished by, for instance, using a material with significantly higher density or by working over a surface where the condensate extends over two materials of different density.

## V. CONCLUSION

In summary, we have performed a precise measurement of the Casimir-Polder force at a significantly larger atom-

surface separation than has previously been achieved. At this large atom-surface separation, effects due to thermal blackbody photons become important, and extension of these measurements to temperatures  $\sim 300$  K above room temperature should allow a clear detection of this effect. Additionally, future experiments performed in nonequilibrium thermal conditions, such as holding the surface at 600 K with the surroundings at 300 K, are predicted to observe significant deviations from the equilibrium thermal Casimir-Polder case [31]. Study of the Casimir-Polder force in such nonequilibrium situations will hopefully permit a better understanding of this often nonintuitive force.

Finally, this experiment has demonstrated promising short-range force sensitivity that could provide limits on Yukawa-type forces utilizing a significantly different measurement type—i.e., atom-bulk vs bulk-bulk. Future work with ultracold atoms near surfaces utilizing this technique and promising atom-interferometry techniques currently being developed, should enable better limits to be set in the 1–10  $\mu\text{m}$  regime.

## VI. ACKNOWLEDGMENTS

We acknowledge useful conversations with Mauro Antezza, Lev Pitaevskii, and Sandro Stringari as well as members of the JILA BEC Collaboration. We would additionally like to thank Simon Kaplan for providing references for the optical properties of our substrate materials. This work was supported by grants from the NSF and NIST and is based upon work supported under the NSF.

- 
- [\*] Present address: Simon Fraser University, Department of Physics, 8888 University Drive, Burnaby, British Columbia, Canada V5A 1S6.
- [†] Quantum Physics Division, National Institute of Standards and Technology.
- [1] H. B. G. Casimir and P. Polder, *Phys. Rev.* **73**, 360 (1948).
- [2] C. I. Sukenik, M. G. Boshier, D. Cho, V. Sandoghdar, and E. A. Hinds, *Phys. Rev. Lett.* **70**, 560 (1993).
- [3] S. K. Lamoreaux, *Phys. Rev. Lett.* **78**, 5 (1997).
- [4] A. Landragin, J. Y. Courtois, G. Labeyrie, N. Vansteenkiste, C. I. Westbrook, and A. Aspect, *Phys. Rev. Lett.* **77**, 1464 (1996).
- [5] F. Shimizu, *Phys. Rev. Lett.* **86**, 987 (2001).
- [6] V. Druzhinina and M. DeKieviet, *Phys. Rev. Lett.* **91**, 193202 (2003).
- [7] Y. J. Lin, I. Teper, C. Chin, and V. Vuletic, *Phys. Rev. Lett.* **92**, 050404 (2004).
- [8] T. A. Pasquini, Y. Shin, C. Sanner, M. Saba, A. Schirotzek, D. E. Pritchard, and W. Ketterle, *Phys. Rev. Lett.* **93**, 223201 (2004).
- [9] H. Oberst, Y. Tashiro, K. Shimizu, and F. Shimizu, *Phys. Rev. A* **71**, 052901 (2005).
- [10] G. Roati, E. de Mirandes, F. Ferlaino, H. Ott, G. Modugno, and M. Inguscio, *Phys. Rev. Lett.* **92**, 230402 (2004).
- [11] Y.-J. Wang, D. Z. Anderson, V. M. Bright, E. A. Cornell, Q. Diot, T. Kishimoto, M. Prentiss, R. A. Saravanan, S. R. Segal, and S. Wu, *Phys. Rev. Lett.* **94**, 090405 (2005).
- [12] M. Saba, T. A. Pasquini, C. Sanner, Y. Shin, W. Ketterle, and D. E. Pritchard, *Science* **307**, 1945 (2005).
- [13] M. Antezza, L. P. Pitaevskii, and S. Stringari, *Phys. Rev. A* **70**, 053619 (2004).
- [14] H. J. Lewandowski, D. M. Harber, D. L. Whitaker, and E. A. Cornell, *J. Low Temp. Phys.* **132**, 309 (2003).
- [15] D. M. Harber, J. M. McGuirk, J. M. Obrecht, and E. A. Cornell, *J. Low Temp. Phys.* **133**, 229 (2003).
- [16] J. M. McGuirk, D. M. Harber, J. M. Obrecht, and E. A. Cornell, *Phys. Rev. A* **69**, 062905 (2004).
- [17] S. Schneider, A. Kasper, C. vom Hagen, M. Bartenstein, B. Engeser, T. Schumm, I. Bar-Joseph, R. Folman, L. Feenstra, and J. Schmiedmayer, *Phys. Rev. A* **67**, 023612 (2003).
- [18] The threshold limit for  $\delta_\gamma$  was defined as the statistical error in  $\gamma_x^{cm}$ . This definition, although somewhat arbitrary, carries significance because if  $\delta_\gamma$  is much larger than the statistical error in  $\gamma_x^{cm}$ , then there is certainly

a significant spatially inhomogeneous force present.

- [19] This is not such an unlikely situation. In our previous work studying alkali adsorbates [16], we measured electric fields from alkali atoms adsorbed onto surfaces. The spatial distribution of atoms that adsorb onto the surface from the condensate will reflect the dimensions of the condensate and thus essentially form an elongated stripe of electrical dipoles collinear to the axis of the condensate.
- [20]  $\partial \vec{B} / \partial t$  due to the charging and discharging of the plates is extremely small and can be safely neglected.
- [21]  $\vec{\nabla} \cdot \vec{B} = 0$  forces the  $\hat{x}$  and  $\hat{y}$  magnetic field gradients to be equal at the center of the trap.
- [22]  $\vec{\nabla} \times \vec{B} \simeq 0$  because we are considering static fields in free space.
- [23] J. Baker-Jarvis, R. G. Geyer, J. H. Grosvenor, Jr., M. D. Janezic, C. A. Jones, B. Riddle, C. M. Weil, J. Krupka, IEEE Trans. Dielectric Electric. Insul. **5**, 571 (1998).
- [24] For calculation of the Casimir-Polder force we utilize the static approximation of [13] that relies only on the DC dielectric constant of the substrate. The static approximation tends to slightly *overestimate* the force in the low-temperature limit. So, for the smaller trap-center to surface separations, the  $T = 0$  K prediction using the full theory would be slightly further below the  $T = 300$  K prediction. The size of this correction for  $T = 300$  K is not enough to shift the limit curve in Fig. 3.
- [25] S. Dimopoulos and A. A. Geraci, Phys. Rev. D **68**, 124021 (2003).
- [26] R. S. Decca, D. Lopez, E. Fischbach, G. L. Klimchitskaya, D. E. Krause, V. M. Mostepanenko, Ann. Phys. (N.Y.) **318**, 37 (2005).
- [27] J. Chiaverini, S. J. Smullin, A. A. Geraci, D. M. Weld, and A. Kapitulnik, Phys. Rev. Lett. **90**, 151101 (2003).
- [28] J. C. Long, H. W. Chan, A. B. Churnside, E. A. Gulbis, M. C. M. Varney, and J. C. Price, Nature **421**, 922 (2003).
- [29] M. Bordag, U. Mohideen, and V. M. Mostepanenko, Phys. Rep. **353**, 1 (2001).
- [30] J. C. Long, H. W. Chan, and J. C. Price, Nucl. Phys. B **539** (1999) 23.
- [31] M. Antezza, L. P. Pitaevskii, and S. Stringari, Phys. Rev. Lett. **95**, 113202 (2005).